PCCP

Accepted Manuscript

ROYAL SOCIETY OF CHEMISTRY

www.rsc.org/pccp

Journal Name

ARTICLE TYPE

Cite this: DOI: 10.1039/xxxxxxxxxx

On the Nature of the Solvated Electron in Ice I_h

Maurice de Koning,[a*] Adalberto Fazzio,[b*] Antônio José Roque da Silva[c*] and Alex Antonelli[a*]

Received Date
Accepted Date

DOI: 10.1039/xxxxxxxxxx

www.rsc.org/journalname

The water-solvated excess electron (EE) is a key chemical agent whose hallmark signature, its asymmetric optical absorption spectrum, continues to be a topic of debate. While nearly all investigation has focused on the liquid-water solvent, the fact that crystalline-water solvated EE shows a very similar visible absorption pattern has remained largely unexplored. Here, we present spin-polarized density-functional theory calculations subject to periodic boundary conditions of the interplay between an EE and a number of intrinsic lattice defects in ice I_h. Our results show that the optical absorption signatures in the presence of three unsaturated hydrogen bonds (HB) are very similar to those observed experimentally. Its low-energy side can be attributed to transitions between the EE ground state and a single localized excited level, in a picture that is different from that for the liquid solvent, where this portion has been associated with hydrogen-like $s \rightarrow p$ excitations. The blue tail, on the other hand, relates to transitions between the EE ground state and delocalized excited states, which is in line with the bound-to-continuum transition interpretations for the EE in liquid water. Finally, we find that, depending on the number of dangling HBs participating in the EE trap, its charge density may spontaneously break the spin degeneracy through exchange interactions with the surrounding electrons, displaying the many-electron quantum nature of the EE problem in ice I_h.

1 Introduction

The name "solvated electron" is given to an excess electron (EE) generated by high-energy ionizing radiation that becomes trapped by a number of molecules of a dipolar solvent such as ammonia or water.[1,2] The water-solvated EE is a particularly important entity that plays a central role in many different settings and has been the subject of intense scrutiny over the past 40 years.[5–35] Its hallmark signature is an asymmetric optical absorption band in the visible range characterized by a broad peak centered around 1.7 eV with Gaussian and Lorentzian-like tails on the red and blue sides of the spectrum, respectively.

In spite of recent alternative ideas,[27–33] the predominant view envisions the water-solvated EE as being localized inside an approximately spherical cavity formed by surrounding water molecules with O-H bonds pointing toward its center.[13–18,22–26] In this perspective the solvated EE system is pictured in terms of a hydrogen-like problem in which the EE occupies an s-type ground-state orbital. The Gaussian part of the absorption profile is thought to be the result of three nearly degenerate $s \rightarrow p$-like transitions between bound states,[16–22] whereas the origin of the slowly decaying blue tail of the spectrum remains an issue of discussion, with some attributing it to excitations to delocalized continuum levels,[18,36] whereas others contend it to involve spatially extended, yet bound EE states.[22]

However, an important issue that relates directly to the physical nature of EE solvation by water molecules has been given very little attention in these discussions. It concerns the comparison between the visible-range EE absorptions for liquid water and that for another water solvent, namely crystalline ice I_h.[37] Experimental data shows that these spectra are very much alike,[12,38] both being characterized by the same shape with Gaussian and Lorentzian-like tails on the red and blue side of the spectrum, respectively. In particular, although the low-energy rise for ice is narrower than for liquid water, the blue tails and peak maxima are essentially identical for both solvents.[12]

The strong similarity of the visible spectra is remarkable given that both the structure as well as the dynamics of the hydrogen-bond (HB) networks in both solvents are manifestly different. In addition to the difference between crystalline and liquid order, the time scale of HB dynamics in ice is orders of magnitude slower than in liquid water. For temperatures close to the melt-

† Electronic Supplementary Information (ESI) available: [Details of considered defect structures, EE characteristics in defect-free ice I_h and absorption properties in VDD trap]. See DOI: 10.1039/b000000x/

[a] *Instituto de Física 'Gleb Wataghin', Universidade Estadual de Campinas, 13083-859, Campinas-SP, Brazil. E-mail: dekoning@ifi.unicamp.br*

[b] *Instituto de Física, Universidade de São Paulo, Caixa Postal 66318, 05315-970, São Paulo-SP, Brazil.*

[c] *Laboratório Nacional de Luz Síncrotron, Caixa Postal 6192, 13083-970, Campinas-SP, Brazil.*

ing point, for instance, the liquid and crystalline water solvents are characterized by Debye relaxation times of $\tau_D \sim 1\times10^{-11}$ and $\tau_D \sim 5\times10^{-5}$ seconds, respectively.[37] In terms of EE solvation this suggests that, while the EE may be able to "carve out" its own solvation structure in the liquid, in ice this is much less likely and EE trapping is expected to occur only at pre-existing defect sites. Given that these defects are specific to ice's crystal structure, the strong resemblance of the visible-range absorption spectra in ice and liquid water is noteworthy.[37] Indeed, in the infrared range there is a distinct difference between the two water phases, with the ice-solvated electron showing an absorption rise that is absent for the liquid solvent.[38]

Despite this experimental insight, however, theoretical studies of the character of the solvated electron in ice have been scarce. Aside from a number of studies considering the EE on the ice surface,[34,35,39,40] there have been few attempts to model the bulk species.[41,42] Shkrob modeled it using a finite ice cluster approach and a mixed QM/MM description,[41] but was unable to capture the asymmetric shape of the optical absorption signature. Bhattacharya and coworkers,[42] on the other hand, carried out fully quantum-mechanical calculations based on density-functional theory (DFT) and periodic boundary conditions but, while reporting on the molecular vacancy EE affinities, did not discuss absorption characteristics.

Here we present results of a study into the interplay between the EE and a variety of intrinsic lattice defects in bulk ice I_h using fully periodic DFT calculations in which all valence electrons are treated on equal footing and explicitly taking into account the spin degrees of freedom of the electrons. This methodology, together with the calculation of the optical absorption signatures in terms of the DFT frequency-dependent dielectric function[43] and the quantification of electron-level localization using criteria from the Theory of Localization,[44] allows us to investigate the correlation between defect- and electronic band structures, the corresponding absorption signature for the EE, as well as the orbital and spin characters of the involved electron states. In addition to revealing environment-dependent spin polarization effects,[45] the results allow us to investigate the nature of the electronic transitions that give rise to the EE visible absorption profile in ice as well as hypothesize on the origin of the similarities and differences in comparison to the case of liquid water.

2 Methodology and Computational details

2.1 DFT Calculations

All calculations are based on plane-wave spin-polarized DFT,[46–48] in which all valence electrons are treated within the Kohn-Sham (KS) scheme.[46–48] We use two different exchange-correlation (XC) functionals: the standard generalized-gradient approximation (GGA) functional of Perdew, Burke and Ernzerhof (PBE),[49] and the hybrid PBE0 functional.[50] The latter contains a part of exact Hartree-Fock (HF) exchange and has been shown to produce chemical accuracy for various systems,[51,52] significantly reducing the spurious self-interaction error (SIE) involved in the systematic band-gap underestimates[53] as well as the unphysical delocalization of unpaired EEs for standard XC functionals.[34,35,42] All calculations are performed using the ab-initio total-energy program Vienna Ab initio Simulation Package (VASP).[54,55] We use the projector augmented-wave (PAW) approach,[56] the Kohn-Sham (KS) orbitals are expanded using plane-wave basis set with a kinetic-energy cutoff of 700 eV and Brillouin-zone sampling is carried out according to the Monkhorst-Pack scheme[57] using grids between $1\times1\times1$ and $5\times5\times5$ k-points. All supercells are based on the defect-free periodic supercell of 96 water molecules generated by Hayward and Reimers and labeled as $3\times2\times2$[58] and lattice parameters that corresponds to the experimental values for ice at 296 K,[37] giving a volume of 3127.95 Å. The optical properties are determined from the independent-particle frequency-dependent dielectric function computed according to the method described in[43]. Prior to the calculation of the optical and localization properties, all ionic configurations are optimized to a level at which the magnitude of the force on each ion is less than 15 meV/Å.

2.2 Quantification of Localization: Participation Ratio

As discussed in the Theory of Localization,[44] the degree of spatial localization of quantum states, electron densities or vibrational modes can be quantified in terms of a quantity known as the *Participation Ratio* (PR).[44,59] Considering, for instance, an electronic density $\rho(r)$ associated with some KS orbital, its Participation Ratio, which has the dimensions of volume, is defined as

$$\mathrm{PR} \equiv \frac{\left[\int_V \rho(r)\mathrm{d}^3r\right]^2}{\int_V \rho^2(r)\mathrm{d}^3r}, \qquad (1)$$

where V is the volume of the computational cell. For instance, if the density is uniform, i.e., $\rho(r) = 1/V$, its PR will be equal to the volume V of the cell, meaning that the spatial extension of this density is V, occupying the entire volume of the cell. For a more localized state, its PR-value will be smaller than V, corresponding to the volume that effectively participates in its extension.

3 Results

3.1 Defect-free Ice I_h

As a first step we compute the optical properties of defect-free ice I_h in the absence of EEs. The results are depicted in Figure 1, which compares experimental data[60,61] to the computed real and imaginary parts of the frequency-dependent dielectric function obtained using $3\times3\times3$ Brillouin-zone sampling and 156 empty KS levels.

The PBE dielectric functions are qualitatively similar to experiment, with the exception of two important elements. In addition to a global red shift with respect to the experimental signature, the PBE absorption profile does not capture the pronounced excitonic peak. As mentioned earlier, the red shift is in part related to the SIE and, as shown in Fig. 1 **A**, the PBE0 hybrid functional significantly reduces this discrepancy. The excitonic peak, on the other hand, cannot be captured within any independent-particle approach and requires explicit treatment of electron-hole interactions, as discussed in detail in Ref. 62.

For the absorption properties of interest here, however, this particular kind of electron-hole interaction is not expected to play a role. In contrast to the band exciton responsible for the excitonic

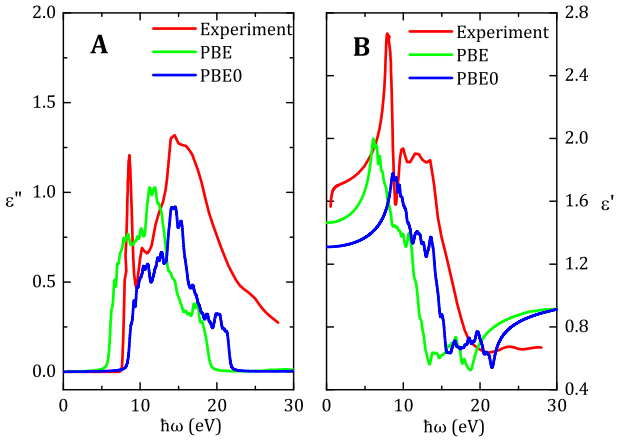

Fig. 1 (**A**) and (**B**) show imaginary and real parts, respectively, of the frequency-dependent dielectric function $\varepsilon(\omega) = \varepsilon'(\omega) + i\varepsilon''(\omega)$ as a function of $\hbar\omega$. Red lines correspond to experimental data from Ref. 60 and 61. Green and blue lines are DFT results based on PBE and PBE0 functionals, respectively.

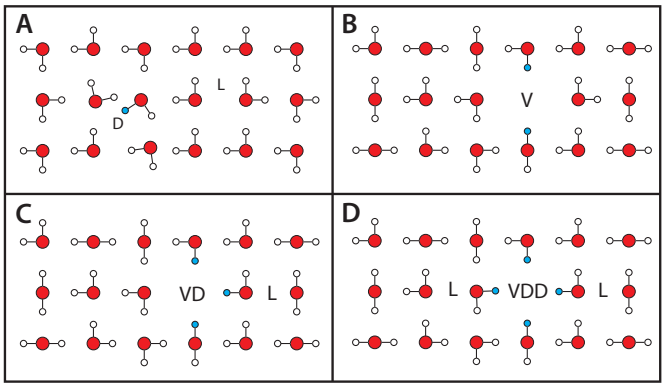

Fig. 2 Schematic HB topologies involved in (A) the D-type Bjerrum defect, (B) the molecular vacancy (V), (C) the VD complex and (D) the VDD structure. Protons associated with dangling HBs are shown in blue and L-type Bjerrum defects are marked with "L". See SI Appendix for further details.

peak in Fig. 1 **A**, the water-solvated excess electrons are generated by high-energy ionizing radiation, typically of the order of MeVs,[2–4] removing electrons from strongly screened atomic core shells rather than from the top of the valence band. Nevertheless, other electron-correlation effects beyond DFT may play a role in the optical absorption properties of the solvated electron in ice, as discussed further below.

3.2 Defects in Ice I_h

Given that the EE is unable to reach a solvated state in the perfect crystal due to the absence of HBs (See SI Appendix for details),[42] the absorption observed experimentally[12,38] is associated with the presence of crystal defects.[4,35,37,41,42,63] Here we consider 4 defect structures that are intrinsic in nature and introduce between 1 and 4 dangling HBs per defect: the D-type Bjerrum defect[37,64] (1 dangling HB), the molecular vacancy (V, 2 HBs)[65] and the complexes formed by combining a vacancy and one D-defect (VD, 3 HBs) as well as the combination of a vacancy and two D-defects (VDD, 4 HBs).[66] Figure 2 illustrates the character of the HB topologies involved in these defect structures in terms of the hypothetical 2-dimensional square ice.[37] Further details are described in the SI Appendix.

The DFT formation energies of Bjerrum defects and the molecular vacancy, as well as the binding energies of their complexes have been reported previously.[64–67] The VD complex is characterized by a positive binding energy of ~ 0.4 eV,[66,67] meaning it is stable with respect to dissociation into an isolated vacancy and D-type Bjerrum defect. The VDD center, on the other hand, is only metastable, being ~ 0.3 eV higher in energy compared to a configuration featuring an isolated VD complex and D-type Bjerrum defect.[68]

Of these we first consider the VD defect, which, based on the pulse ionization experiments on NH_3-doped ice,[4,37] has been anticipated to play a particularly important role as a trapping center for the EE. Fig. 3 shows a typical DFT charge-density profile as well as corresponding absorption profiles for the EE in the presence of a VD defect complex. The first observation is that the EE density is strongly localized within the vacancy cavity with a three-fold symmetric pattern that reflects the 3 dangling HBs. Quantifying the localization in terms of the Participation Ratio (PR) (see Materials and Methods), the EE density for the PBE functional effectively occupies a volume of ~ 1.4 times that of a 12-molecule cage of the ice I_h structure, which is equivalent to the volume of a sphere of radius ~ 3 Å. Indeed, this degree of localization is comparable to the typical radii of gyration reported for the solvated EE ground state in liquid water,[23,24,69] which suggests that the EE ground-state electron densities in both solvents are similar. The PBE0 hybrid functional increases the localization by 20%, reducing the participating volume to ~ 1.1 times that of a 12-molecule cage or a localization radius of ~ 2.8 Å.

Furthermore, the EE charge density is found to be spin polarized for both functionals, in the sense that the degeneracy of the KS levels associated with both spin projections is lifted. This effect is a direct manifestation of the many-electron quantum nature of the EE problem in ice I_h and is caused by exchange interactions between the localized EE and the electrons in the surrounding water molecules.[45] As discussed below, its appearance correlates with the number of dangling protons available in the solvation structure.

Considering the DFT absorption profiles, their quantitative features, such as peak position and widths, clearly depend on the particular functional. The PBE band is narrower and has its peak position located at lower energies compared to experi-

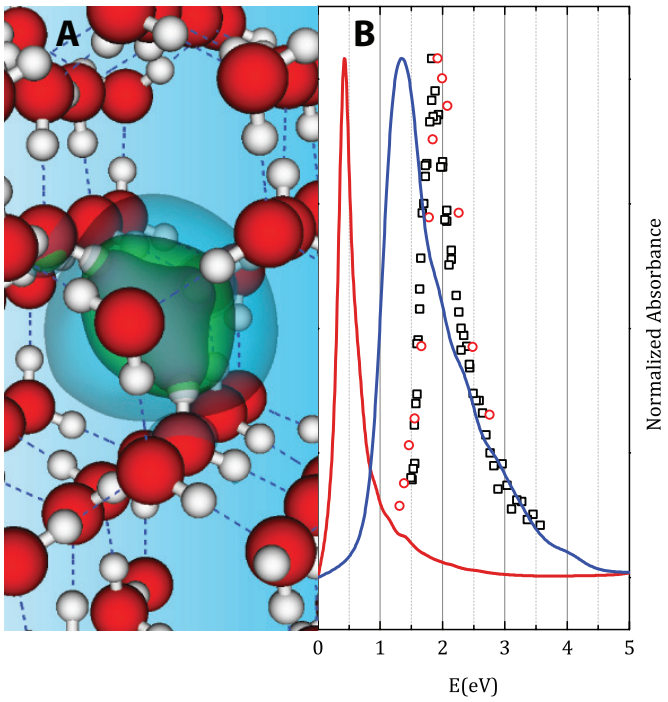

Fig. 3 Typical total charge-density profile and absorption signals for the EE in the presence of a VD defect complex. (**A**) shows PBE charge-density profile for 5x5x5 Brillouin-zone sampling obtained by subtracting both spin-component total electron densities. Three contours depict density levels of 1.6×10^{-2}, 9×10^{-3}, and 1.6×10^{-3} $e/\text{Å}^3$. (**B**) shows normalized absorption profiles for PBE and PBE0 functionals, as well as experimental data. Red and blue lines represents 5x5x5 PBE and 3x3x3 PBE0 absorptions, respectively. Squares and circles depict the experimental results from Refs.[12] and[38], respectively.

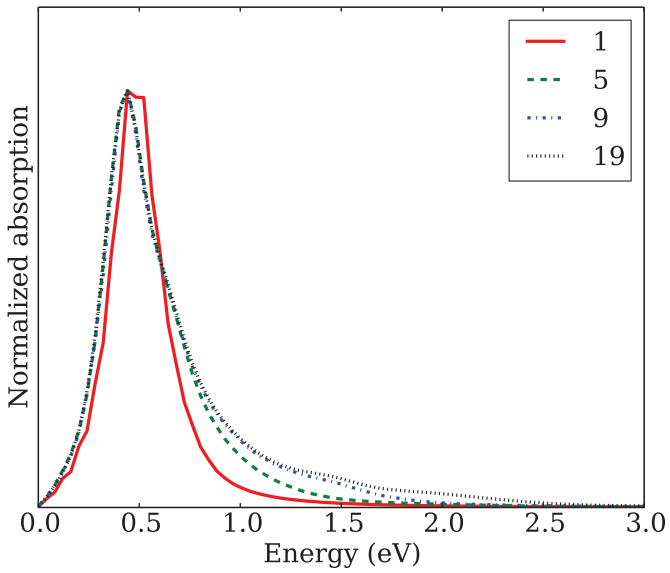

Fig. 4 Emergence of asymmetric absorption profile for the EE in the presence of the VD defect as a function of the number of unoccupied states in the optical response calculation for the PBE functional. Results correspond to cases including 1 (full line), 5 (dashed line), 9 (dot-dashed line) and 19 empty states (dotted line), respectively.

ment, mostly due to the self-interaction error (SIE) characteristic for standard GGA exchange-correlation functionals. Indeed, when performing the calculations using the PBE0 hybrid functional, which is known to substantially reduce the SIE,[34,35,53] the peak location and width become closer to the experimental values. Even so, to obtain quantitatively accurate peak properties electron-correlation effects that go beyond DFT, such as appropriately accounting for quasi-particle self-energies and explicitly including electron-hole interactions, must be considered.[70–72] Unfortunately, calculation of these contributions is currently prohibitively costly for the systems considered here. Nevertheless, given that the self-energy and electron-hole contributions lead to energy corrections with opposite signs and the fact that the DFT absorption profiles are qualitatively very similar to those seen in the experiments, as discussed below, it is expected that a DFT-level description is able to provide useful insight into the absorption characteristics of the solvated electron in ice.

As shown in Fig. 3 **B** the qualitative shape of the absorption bands is the same for the two functionals, both displaying the characteristic asymmetric form observed in experiment, featuring a fast rise on the red side and a slow decay on the blue side. To rationalize the origin of this form, we compute the optical absorption response for the EE in the VD defect using different numbers of unoccupied states in the calculation. The self-consistent electron density was first determined using a $5\times5\times5$ grid and the corresponding dielectric response for this density was subsequently computed using a $9\times9\times9$ k-point grid including increasing numbers of unoccupied levels. Because of the prohibitively large RAM memory requirements for PBE0 using these k-point grids, the calculations were carried out only for the PBE functional. The results are shown in Fig. 4, which shows the absorption profiles for 1, 5, 9 and 19 empty KS levels, respectively.

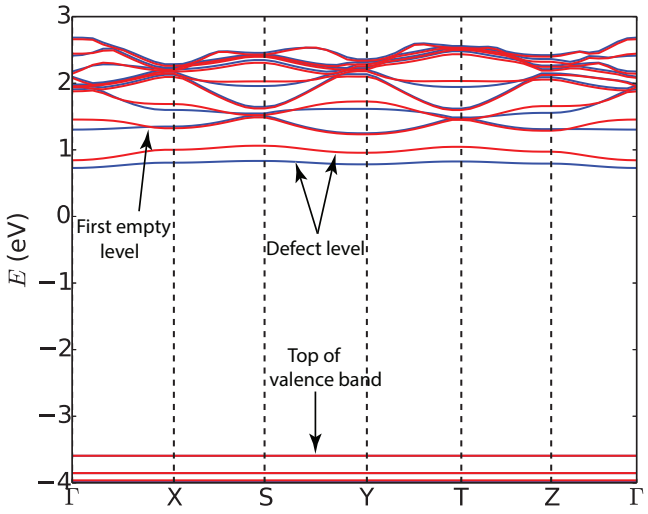

Fig. 5 Spin-polarized Kohn-Sham band structure for ice I_h in the presence of a VD defect computed for the PBE functional and $5 \times 5 \times 5$ k-point electron density. Blue and red lined represent the two spin components. Defect level displays distinct spin polarization.

Taking into account only one empty state gives a profile that is essentially symmetric, whereas inclusion of more unoccupied levels leads to a progressively more asymmetric form that converges when ~ 9 empty states are taken into account. The finite width of the absorption profile for a single unoccupied level is caused by the dispersion of the empty KS states, which is depicted in Fig. 5. It shows the PBE spin-polarized KS band structure for the system with the VD defect along the path Γ-X-S-Y-T-Z-Γ in the Brillouin zone associated with the simulation cell. The valence bands shown on the bottom are entirely flat, reflecting the fact that these correspond to the very strongly localized electron states associated with the covalent O-H bonds and the lone pairs of the water molecules. The EE ground-state level also shows little dispersion due to its localization, but it is spin polarized with both spin components separated by 0.1-0.2 eV throughout. On the other hand, as previously noted,[73] the empty states show progressively more dispersion, which leads to the finite-width absorption profile even when only a single unoccupied level is taken into account.

The increasing degree of dispersion is also reflected in the trend of the PR values for the first few unoccupied states. Whereas the EE ground state effectively occupies a volume equivalent to that of a sphere of radius ~ 3 Å, the first unoccupied KS level is spread over three times this volume. The next two empty levels become even more delocalized, with PR values 7-9 times larger than that of the ground state. This progressive delocalization can be further illustrated by visualizing charge-density contours associated with these 4 spin states, as shown in Fig. 6. The ground-state level and the first excited state retain localization in the vicinity of the defect level, but the next two empty states display typical conduction-band character, being strongly delocalized and effectively detached from the trapping site.

The above results indicate that the low-energy Gaussian-like part of the absorption for the VD center for ice is linked to a transition between the ground-state level and a single localized excited state, whereas transitions to higher-lying continuum-like states are responsible for the slowly decaying blue tail. Although similar in general terms, with the red portion of the spectrum being associated with transitions between localized bound EE states and the blue tail involving transitions to delocalized levels, the specific characteristics are markedly different from the case of the liquid solvent. In particular, while the low-energy feature in the latter has been attributed to hydrogen-like transitions between an s-type ground state and three nearly degenerate localized p-type excited levels,[16–22] for the VD center it involves a single transition between two localized states that do not exhibit hydrogen-like structure.

Starting from the VD complex, an even stronger trapping site may be created, in principle, by adding a second D-type Bjerrum defect. The resulting VDD center supplies four inward-pointing HBs and, as detailed in the SI Appendix, it indeed leads to a more strongly localized spin-polarized EE density. On the other hand, compared to that of the VD center, its equilibrium concentration is expected to be negligible because of its tendency to dissociate into a VD complex and an isolated D defect, as mentioned above.

Finally, we consider the D-type Bjerrum defect and molecular vacancy centers, which supply 1 and 2 dangling HBs, respectively. Fig. 7 shows typical charge-densities as well as the corresponding absorption profiles. In both cases, the localization is significantly diminished compared to the VD complex, with occupied volumes $\sim$10 times that of a 12-molecule cage or a radius of $\sim$6 Å and the EE charge densities are no longer spin polarized. As a result, both centers are weaker trapping sites and this is reflected in the absorption signatures, both of which are in the infrared range, with the PBE and PBE0 peaks around 0.25 eV and 0.7 eV, respectively. As for the VD complex, the asymmetry of both profiles is linked to the dispersion of the conduction band states. In line with previous calculations,[41] this finding is consistent with the existence of an infrared absorption rise for the EE in ice,[38] as shown in Fig. 7, that is absent in liquid water. The reason for this absence in the liquid phase remains an open question, but it may possibly be related to the vastly different HB relaxation time scales in both solvents. While in ice few-dangling-HB centers such as the D-defect and the molecular vacancy are stable,[64,65] in the liquid phase such configurations may be too short-lived, even in the presence of an EE.

4 Discussion

We have carried out a spin-polarized DFT study of the interplay between the EE and a variety of intrinsic lattice defects in bulk ice I_h involving different numbers of dangling hydrogen bonds. Our approach is based on a homogeneous description in which all valence electrons in the system are treated on equal footing and we apply periodic boundary conditions to minimize surface effects. We find that the VD trapping center with three dangling HBs produces a localized EE ground state level that gives a broad visible optical absorption signature with position and shape very much alike that seen in the experimental visible-range spectra for both ice and liquid water. Defect centers providing one and two HBs, on the other hand, give absorption features in the infrared range.

Considering the particular character of the electronic states in-

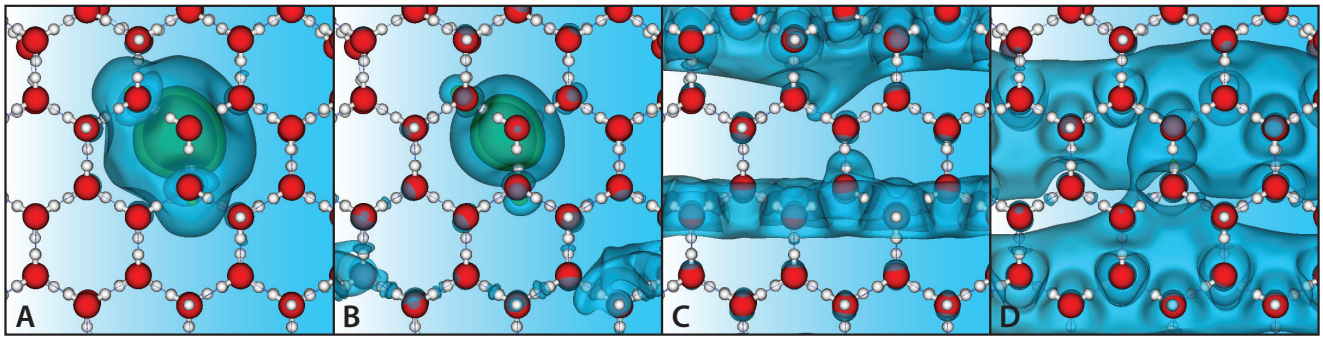

Fig. 6 Electron density contour levels associated with KS spin states in the presence of a VD defect. Shown levels correspond to electron densities of 6.4×10^{-3}, 3.5×10^{-3} and 6.4×10^{-4} $e/\text{Å}^3$. (**A**) KS ground-state spin orbital occupied by EE. (**B**), (**C**) and (**D**) display charge densities for first three excited KS levels.

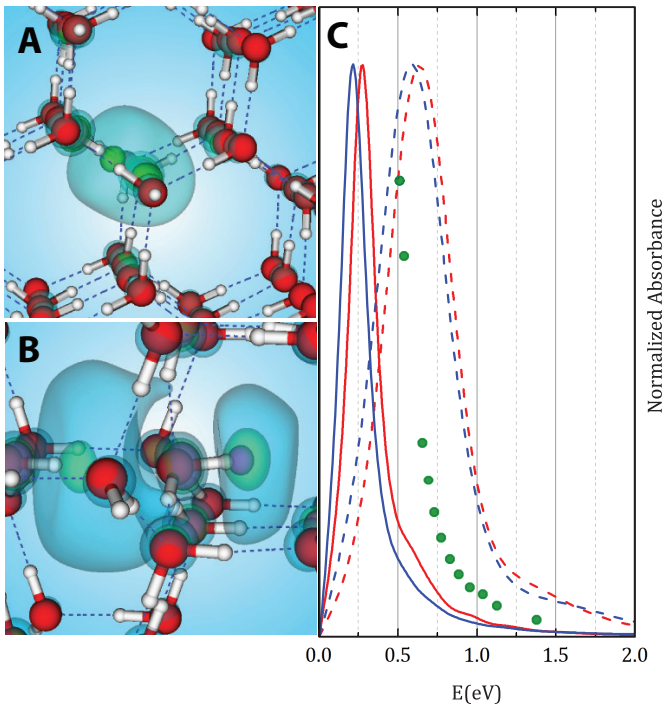

Fig. 7 Typical charge-density profile and absorption signals for the EE in the presence of a molecular vacancy and a D-type defect complex. (**A**) and (**B**) show PBE charge-density profile associated with the Kohn-Sham orbital occupied by the EE in the presence of the molecular vacancy and the D-type Bjerrum defect, respectively. Three contours depict density levels of 1.6×10^{-2}, 1.0×10^{-2}, and 3.2×10^{-3} $e/\text{Å}^3$. (**C**) shows normalized absorption profiles for PBE (full lines) and PBE0 functionals (dashed lines), for the molecular vacancy (blue lines) and the D-type Bjerrum defect (red lines). Green circles depict experimental infrared absorption from Ref. 38.

volved in the low-energy side of the visible absorption, we find a scenario that is different from that for the liquid solvent. Instead of a hydrogen-like picture involving three excitations between an *s*-type ground state and three almost *p*-type states, for the VD center in ice it is the result of a transition to a single localized unoccupied level. On the other hand, despite this particular difference, the fact that both cases involve electronic states that retain substantial localization in the vicinity of the solvation site is an indication that this portion of the absorption signature is a reflection of the local structure of the EE solvation geometry. In this perspective, it is possible that the experimentally observed difference between liquid water and ice for this portion of the absorption signature [12] is in fact a manifestation of different solvation motifs in both solvents. Indeed, while in liquid water the number of involved unsaturated HBs is thought to range between four and six, [13,16,19,21,25] our present results for ice indicate a structure with only three.

One may also hypothesize as to why the blue absorption tails in ice and liquid water are so much alike, in contrast to the low-energy part. Our results for the VD center in ice show that this portion of the absorption profile can be attributed to excitations between the solvated EE ground-state level and delocalized excited states, and this is in line with the bound-to-continuum transition interpretation for the liquid phase. [18,36] This then suggests that, for both solvents, this part of the spectrum is largely controlled by the character of bulk-like conduction-band levels that are essentially decoupled from the solvation structure. Both theoretical [73] as well as experimental evidence [74] indicates that the bulk electronic structures of liquid water and ice are strongly resemblant and it seems plausible that this proximity is key to the resemblance between the high-energy parts of the visible EE absorption in both solvents.

Finally, an observation that pertains to the general nature of EE solvation in condensed phases of water is that, depending on the number of available dangling protons involved in the trap, the EE charge density may spontaneously lift the spin degeneracy due to exchange-interaction effects. In ice this occurs for the VD and VDD defect complexes, which provide 3 and 4 unsaturated HBs, respectively, and it is a direct manifestation of the many-electron quantum nature of the EE problem in ice I_h. Indeed, the fact that this degeneracy is not broken for the D-type Bjerrum defect

and the molecular vacancy is an indication of the direct relation between solvation structure and the importance of such effects, which may also be relevant for the case of EE solvation in liquid water.

Acknowledgement

The authors gratefully acknowledge financial support from the Brazilian agencies Fapesp, CNPq and Capes and the Center for Computational Engineering and Sciences - Fapesp/Cepid no. 2013/08293-7. The calculations were carried out at CCJDR-IFGW-UNICAMP.

References

1 W. Weyl, *Ann. Phys.*, 1864, **197**, 601–612.
2 E. J. Hart and J. W. Boag, *J. Am. Chem. Soc.*, 1962, **84**, 4090–4095.
3 J. M. Warman, M. P. De Haas and J. B. Verberne, *J. Phys. Chem.*, 1980, **84**, 1240–1248.
4 M. Kunst, J. M. Warman, M. P. De Haas and J. B. Verberne, *J. Phys. Chem.*, 1983, **87**, 4096–4098.
5 B. Michael, E. Hart and K. Schmidt, *J. Phys. Chem.*, 1971, **75**, 2798–2805.
6 F.-Y. Jou and G. R. Freeman, *J. Phys. Chem.*, 1979, **83**, 2383–2387.
7 H. Christensen and K. Sehested, *J. Phys. Chem.*, 1986, **90**, 186–190.
8 T. R. Tuttle and S. Golden, *J. Phys. Chem.*, 1991, **95**, 5725–5736.
9 L. Turi and P. J. Rossky, *Chem. Rev.*, 2012, **112**, 5641–5674.
10 B. Abel, U. Buck, A. L. Sobolewski and W. Domcke, *Phys. Chem. Chem. Phys.*, 2012, **14**, 22–34.
11 D. M. Bartels, K. Takahashi, J. A. Cline, T. W. Marin and C. D. Jonah, *J. Phys. Chem. A*, 2005, **109**, 1299–1307.
12 Y. Du, E. Price and D. M. Bartels, *Chem. Phys. Lett.*, 2007, **438**, 234–237.
13 L. Kevan, *Acc. Chem. Res.*, 1981, **14**, 138–145.
14 A. Wallqvist, G. Martyna and B. J. Berne, *J. Phys. Chem.*, 1988, **92**, 1721–1730.
15 M. Boero, M. Parrinello, K. Terakura, T. Ikeshoji and C. C. Liew, *Phys. Rev. Lett.*, 2003, **90**, 226403–.
16 J. Schnitker and P. J. Rossky, *J. Chem. Phys.*, 1987, **86**, 3462–3470.
17 J. Schnitker, K. Motakabbir, P. J. Rossky and R. A. Friesner, *Phys. Rev. Lett.*, 1988, **60**, 456–459.
18 P. J. Rossky and J. Schnitker, *J. Phys. Chem.*, 1988, **92**, 4277–4285.
19 L. Turi and D. Borgis, *J. Chem. Phys.*, 2002, **117**, 6186–6195.
20 L. D. Jacobson, C. F. Williams and J. M. Herbert, *J. Chem. Phys.*, 2009, **130**, 124115.
21 L. D. Jacobson and J. M. Herbert, *J. Chem. Phys.*, 2010, **133**, 154506.
22 L. D. Jacobson and J. M. Herbert, *J. Am. Chem. Soc.*, 2010, **132**, 10000–10002.
23 O. Marsalek, F. Uhlig, T. Frigato, B. Schmidt and P. Jungwirth, *Phys. Rev. Lett.*, 2010, **105**, 043002–.
24 O. Marsalek, F. Uhlig, J. VandeVondele and P. Jungwirth, *Acc. Chem. Res.*, 2012, **45**, 23–32.
25 J. M. Herbert and L. D. Jacobson, *Int. Rev. Phys. Chem.*, 2011, **30**, 1–48.
26 F. Uhlig, J. M. Herbert, M. P. Coons and P. Jungwirth, *J. Phys. Chem. A*, 2014, **118**, 7507–7515.
27 R. E. Larsen, W. J. Glover and B. J. Schwartz, *Science*, 2010, **329**, 65–69.
28 R. Ludwig and D. Paschek, *ChemPhysChem*, 2011, **12**, 75–77.
29 L. Turi and Á. Madarász, *Science*, 2011, **331**, 1387.
30 R. E. Larsen, W. J. Glover and B. J. Schwartz, *Science*, 2011, **331**, 1387.
31 J. R. Casey, A. Kahros and B. J. Schwartz, *J. Phys. Chem. B*, 2013, **117**, 14173–14182.
32 J. R. Casey, R. E. Larsen and B. J. Schwartz, *Proc. Natl. Acad. Sci. U.S.A.*, 2013, **110**, 2712–2717.
33 L. Turi, *J. Chem. Theory Comput.*, 2015, **11**, 1745–1755.
34 F. Baletto, C. Cavazzoni and S. Scandolo, *Phys. Rev. Lett.*, 2005, **95**, 176801–.
35 S. K. Bhattacharya, J. M. Finn, V. P. Diep, F. Baletto and S. Scandolo, *Phys. Chem. Chem. Phys.*, 2010, **12**, 13034–13036.
36 L. Turi, G. Hantal, P. J. Rossky and D. Borgis, *J. Chem. Phys.*, 2009, **131**, 024119.
37 V. F. Petrenko and R. W. Whitworth, *Physics of ice*, Oxford University Press, New York, 1999.
38 H. A. Gillis and T. I. Quickenden, *Can. J. Chem.*, 2001, **79**, 80–93.
39 A. Hermann, P. Schwerdtfeger and W. G. Schmidt, *J. Phys.: Condens. Matter*, 2008, **20**, 225003–.
40 U. Bovensiepen, C. Gahl, J. Stähler, M. Bockstedte, M. Meyer, F. Baletto, S. Scandolo, X.-Y. Zhu, A. Rubio and M. Wolf, *J. Phys. Chem. C*, 2008, **113**, 979–988.
41 I. A. Shkrob, *Chem. Phys. Lett.*, 2007, **443**, 289–292.
42 S. K. Bhattacharya, F. Inam and S. Scandolo, *Phys. Chem. Chem. Phys.*, 2014, **16**, 3103–3107.
43 M. Gajdoš, K. Hummer, G. Kresse, J. Furthmüller and F. Bechstedt, *Phys. Rev. B*, 2006, **73**, 045112–.
44 D. Thouless, *Phys. Rep.*, 1974, **13**, 93–142.
45 T. Clark and G. Illing, *J. Am. Chem. Soc.*, 1987, **109**, 1013–1020.
46 E. Engel and R. Dreizler, *Density Functional Theory: An Advanced Course*, Springer, 2011, pp. –.
47 J. Kohanoff, *Electronic Structure Calculations For Solids And Molecules: Theory And Computational Methods*, Cambridge University Press, 2006, pp. –.
48 R. M. Martin, *Electronic Structure: Basic Theory and Practical Methods*, Cambridge University Press, Cambridge, 2004.
49 J. P. Perdew, K. Burke and M. Ernzerhof, *Phys. Rev. Lett.*, 1996, **77**, 3865–.
50 C. Adamo and V. Barone, *J. Chem. Phys.*, 1999, **110**, 6158–6170.
51 C. Adamo, G. E. Scuseria and V. Barone, *J. Chem. Phys.*, 1999,

111, 2889–2899.
52 L.-L. Wang and D. D. Johnson, *J. Phys. Chem. B*, 2005, **109**, 23113–23117.
53 Y. Zhao and D. G. Truhlar, *J. Chem. Phys.*, 2009, **130**, 074103–3.
54 G. Kresse and J. Furthmüller, *Phys. Rev. B*, 1996, **54**, 11169–11186.
55 G. Kresse and J. Furthmüller, *Comp. Mater. Sci.*, 1996, **6**, 15–50.
56 G. Kresse and D. Joubert, *Phys. Rev. B*, 1999, **59**, 1758–1775.
57 H. J. Monkhorst and J. D. Pack, *Phys. Rev. B*, 1976, **13**, 5188–5192.
58 J. A. Hayward and J. R. Reimers, *J. Chem. Phys.*, 1997, **106**, 1518–1529.
59 R. J. Bell and P. Dean, *Discuss. Faraday Soc.*, 1970, **50**, 55–61.
60 S. G. Warren, *Appl. Opt.*, 1984, **23**, 1206–1225.
61 T. Matsuoka, S. Fujita and S. Mae, *J. Appl. Phys.*, 1996, **80**, 5884–5890.
62 P. H. Hahn, W. G. Schmidt, K. Seino, M. Preuss, F. Bechstedt and J. Bernholc, *Phys. Rev. Lett.*, 2005, **94**, 037404–.
63 M. P. de Haas, M. Kunst, J. M. Warman and J. B. Verberne, *J. Phys. Chem.*, 1983, **87**, 4089–4092.
64 M. de Koning, A. Antonelli, A. J. R. da Silva and A. Fazzio, *Phys. Rev. Lett.*, 2006, **96**, 075501.
65 M. de Koning, A. Antonelli, A. J. R. da Silva and A. Fazzio, *Phys. Rev. Lett.*, 2006, **97**, 155501.
66 M. de Koning and A. Antonelli, *J. Chem. Phys.*, 2008, **128**, 164502.
67 M. de Koning and A. Antonelli, *J. Phys. Chem. B*, 2007, **111**, 12537.
68 M. de Koning and A. Antonelli, unpublished.
69 F. Uhlig, O. Marsalek and P. Jungwirth, *J. Phys. Chem. Lett.*, 2012, **3**, 3071–3075.
70 M. Bockstedte, A. Marini, O. Pankratov and A. Rubio, *Phys. Rev. Lett.*, 2010, **105**, 026401–.
71 P. Rinke, A. Schleife, E. Kioupakis, A. Janotti, C. Rödl, F. Bechstedt, M. Scheffler and C. G. Van de Walle, *Phys. Rev. Lett.*, 2012, **108**, 126404–.
72 F. Karsai, P. Tiwald, R. Laskowski, F. Tran, D. Koller, S. Gräfe, J. Burgdörfer, L. Wirtz and P. Blaha, *Phys. Rev. B*, 2014, **89**, 125429–.
73 D. Prendergast, J. C. Grossman and G. Galli, *J. Chem. Phys.*, 2005, **123**, 014501.
74 D. Nordlund, M. Odelius, H. Bluhm, H. Ogasawara, L. Petterson and A. Nilsson, *https://escholarship.org/uc/item/8vb868t7*, 2008.